

Evaporation, infiltration and storage of soil water in different vegetation zones in the Qilian Mountains: A stable isotope perspective

Guofeng Zhu^{1,2}, Leilei Yong^{1,2}, Xi Zhao^{1,2}, Yuwei Liu^{1,2}, Zhuanxia Zhang^{1,2}, Yuanxiao Xu^{1,2}, Zhigang Sun^{1,2}, Liyuan Sang^{1,2}, Lei Wang^{1,2}

¹ College of Geography and Environment Science, Northwest Normal University, Lanzhou 730070, China

² Shiyang River Ecological Environment Observation Station, Northwest Normal University, Lanzhou 730070, Gansu, China

Correspondence to: Guofeng Zhu (zhugf@nwnu.edu.cn)

Abstract: The processes of water storage have not been fully understood in different vegetation zones in mountainous areas, which is the main obstacle to further understanding hydrological processes and improving water resource assessments. To further understand the process of soil water movement in different vegetation zones (alpine meadow, coniferous forest, mountain grassland, and deciduous forest) in mountainous areas, this study monitored the temporal and spatial dynamics of hydrogen and oxygen stable isotopes in the precipitation and soil water of the Xiyang River Basin. The results show that the order of soil water evaporation intensities in the four vegetation zones was mountain grassland (SWL_{slop} : 3.4) > deciduous forest (SWL_{slop} : 4.1) > coniferous forest (SWL_{slop} : 4.7) > alpine meadow (SWL_{slop} : 6.4). The soil water in the alpine meadow and coniferous forest evaporated from only the topsoil, and the rainfall input was fully mixed with each layer of soil. The evaporation signals of the mountain grassland and deciduous forest could penetrate deep into the middle, and lower layers of the soil as precipitation quickly flowed into the deep soil through the soil matrix. Each vegetation zone water storage capacity of the 0-40 cm soil layer followed the order of alpine meadow (46.9 mm) > deciduous forest (33.0 mm) > coniferous forest (32.1 mm) > mountain grassland (20.3 mm). In addition, the 0-10cm soil layer has the smallest soil water storage capacity (alpine meadow: 43.0 mm; coniferous forest: 28.0 mm; mountain grassland: 17.5 mm; deciduous forest:

30 29.1 mm). This work will provide a new reference for understanding soil hydrology in
31 arid headwater areas.

32 **Key words:** Xiying River; Stable isotope; Drought, Soil water storage

33 **1. Introduction**

34 In arid inland river basins, climate and vegetation changes will affect the
35 hydrological cycle (Sharma et al., 2021; Tetzlaff et al., 2013). As an essential part of
36 the water cycle, soil water in the unsaturated zone can be converted from precipitation
37 into the stream or groundwater recharge. Determining soil water's evaporation,
38 infiltration, and storage properties are critical to understand the regional hydrological
39 cycle and water balance under climate and vegetation changes (Brooks et al., 2010;
40 Dubbert and Werner, 2019; Grant and Dietrich, 2017).

41 As "fingerprints" of water, isotopes have been used to track ecohydrological
42 characteristics, such as evaporation (Barnes and Allison, 1988; Zhu et al., 2021b),
43 groundwater recharge (Koeniger et al., 2016), infiltration paths (Duvert et al., 2016;
44 Tang and Feng, 2001; Zhu et al., 2021a), evapotranspiration distribution (Gibson et al.,
45 2021; Xiao et al., 2018), and the water absorption by plants (Rothfuss and Javaux,
46 2017).

47 Water seepage in the unsaturated soil zone and water evaporation at the air–soil
48 interface are the primary forms of soil water transport. The dynamic water process
49 reflected by the displacement of the isotope signal on the soil profile is called the
50 "memory effect". Understanding the "memory effect" will help us to trace the
51 dynamic changes in climate and soil hydrology (Kleine et al., 2020). The change of
52 stable isotopes in near-surface soil water may reflect the precipitation variation, but
53 these variations decrease with depth unless there is preferential flow (Peralta-Tapia et
54 al., 2015; Sprenger et al., 2016; Sprenger et al., 2017). Evaporation mainly occurred
55 in the near-surface part of the soils (0-10 cm), and the light isotope molecules (^1H and
56 ^{16}O) evaporated preferentially, resulting in the enrichment of heavy isotopes (^2H and
57 ^{18}O) on the soil surface (Ferretti et al., 2003). Dansgaard (1964) proposed the concept
58 of d-excess ($\text{d-excess}=\delta^2\text{H}-8\delta^{18}\text{O}$) to illustrate the intensity of evaporation

59 fractionation. Assuming that evaporation occurs in the atmosphere with a humidity of
60 75%, it shows that the d-excess value of atmospheric moisture accounts for the
61 d-excess value of 10‰ in the atmospheric moisture, which conforms to the worldwide
62 average isotopic labelling of meteoric waters. Landwehr and Coplen (2006) defined
63 line conditioned excess as the difference between the $\delta^2\text{H}$ value of the water sample
64 and the $\delta^{18}\text{O}$ linear transform value of the same sample, where the linear
65 transformation reflects the relevant referenced meteoric water relationship. Compared
66 with d-excess, lc-excess can explain the evaporative fractionation process better. The
67 main reason is that lc-excess of precipitation and soil water changes smoothly and has
68 relatively small seasonal changes (Landwehr et al., 2014). The dynamic changes of
69 isotopes record the signal of soil water evaporation. This enrichment of this dynamic
70 fractionation exists in soil water isotopes in different climatic regions. Compared with
71 temperate regions, the evaporation signals in arid and Mediterranean environments
72 penetrate deeper into the soil (Sprenger et al., 2016). After evaporation and seepage,
73 some water is stored in the soil . The water storage capacity in humid areas is higher
74 than that in arid areas, that in forest is higher than that in grassland, and that in surface
75 soil layer is lower than that in deep soil layers with high clay content (Kleine et al.,
76 2020; Milly, 1994; Snelgrove et al., 2021; Sprenger et al., 2019).

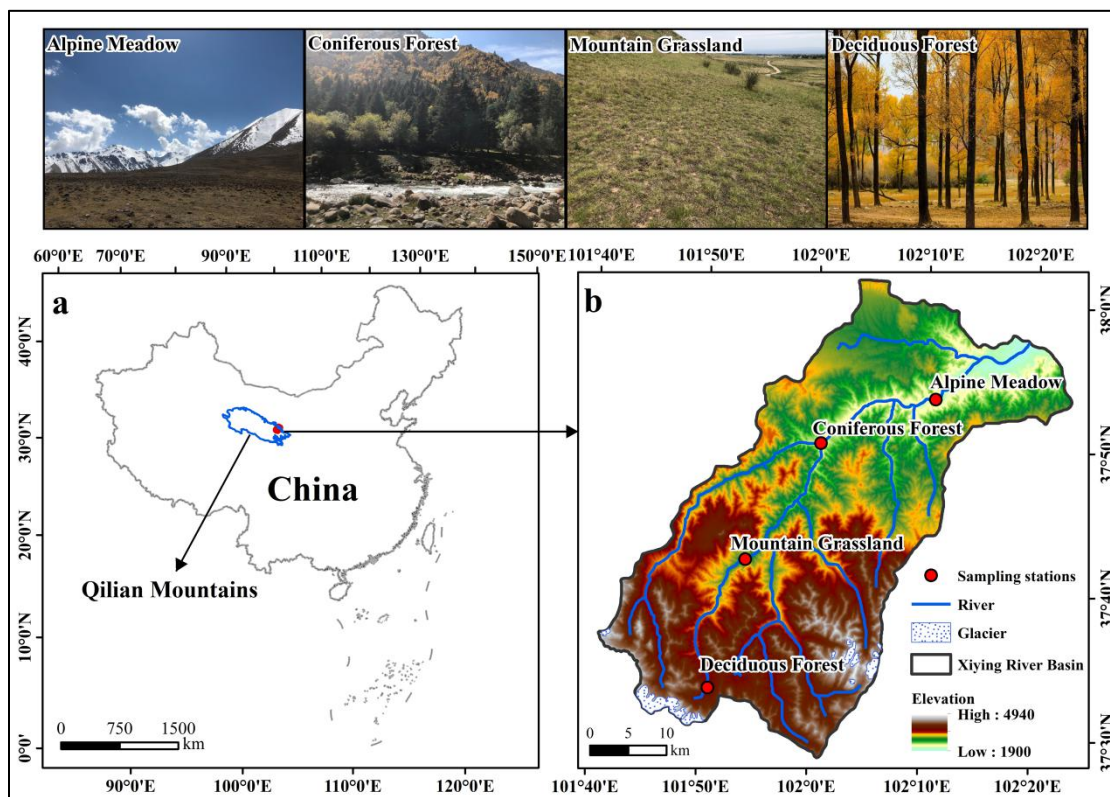
77 In alpine mountains, climate warming has accelerated the melting of glaciers and
78 frozen soil, and the dynamic interaction between water bodies stored in different
79 media has become the main influencing factor of the water cycle (Penna et al., 2018).
80 Interactions between precipitation and the soil-plant-atmosphere system determine the
81 distribution of water in various storage reservoirs and the subsequent release of water
82 vapor to the atmosphere. These interactions include mainly interception, throughfall,
83 canopy drip, snow accumulation and ablation, infiltration, surface and subsurface
84 runoff, soil moisture, and the partitioning of evapotranspiration between canopy
85 evaporation, transpiration, and soil evaporation. As the main links of the hydrological
86 cycle, these processes have a profound impact on regional water balance and
87 distribution.

88 In the past, studies on the evaporation, infiltration and storage of soil water mostly
89 focused on vegetation types in the same climatic region or different climatic regions.
90 Understanding the climatic and hydrological conditions of different vertical
91 vegetation zones and clarifying the regulating role of vegetation in the water cycle can
92 help better adapt to climate change's influences on the hydrological cycle in source
93 areas. In this study, we monitored the stable isotope composition of precipitation and
94 soil water and the spatio-temporal dynamics of soil water storage in four vegetation
95 zones (alpine meadow, coniferous forest, mountain grassland, and deciduous forest) at
96 different temperature and humidity in the Xiyang River basin. To explore the
97 differences in soil water evaporation, infiltration, and storage processes in these four
98 different climates, vegetation types, and terrain types, the following research
99 objectives were proposed: (1) to explore the evolution of isotope evaporation signals
100 and the "memory effects" of precipitation input, mixing and rewetting; (2) to
101 understand the soil water storage capacity and influencing factors of four vegetation
102 areas in mountainous areas. We hope this study can further improve the understanding
103 of the water cycle process and provide a scientific theoretical reference for water
104 resource utilization and ecological restoration in fragile environments. More
105 importantly, it can provide paradigms for research at different spatial scales (latitude
106 zone, longitude zone, watershed, etc.) based on the knowledge of soil moisture
107 evaporation, infiltration, and water storage in mountain vegetation zones.

108 **2. Study area**

109 The Xiyang River originates from Lenglongling and Kawazhang in the eastern
110 Qilian Mountains ($101^{\circ}40'47''\sim 102^{\circ}23'5''E$, $37^{\circ}28'22''\sim 38^{\circ}1'42''N$) (Fig. 1). As
111 the largest tributary of the Shiyang River, it is formed by the Shuiguan River,
112 Ningchang River, Xiangshui River, and Tatu River converging from southwest to
113 northeast and ultimately flowing into the Xiyang Reservoir. The average annual runoff
114 of the Xiyang River is 388 million m^3 , which is mainly replenished by mountain
115 precipitation and melting water of ice and snow. The runoff is mainly concentrated in
116 summer. The basin elevation is between 2000 m and 5000 m, corresponding to a

117 temperate semiarid climate with strong solar radiation, a long sunshine time, and a
 118 large temperature difference between day and night. The average annual temperature
 119 of the basin is 6°C, the annual average evaporation is 1133 mm, the annual average
 120 precipitation is 400 mm, and the precipitation from June to September accounts for
 121 69% of the annual precipitation. Precipitation increases with elevation, while
 122 temperature decreases with elevation in this area (Table 1) (Ma et al., 2018). The
 123 zonal differentiation of vegetation in the basin is dominated by deciduous forest,
 124 mountain grassland, cold temperate coniferous forest, and alpine meadow. The soils
 125 mainly include lime, chestnut, alpine shrub meadow, and desert soil (Fig. 1).



126
 127 **Fig. 1** Study area and location of sampling points (a. The location of the Xiying
 128 River Basin in China; b. The terrain and sampling points of the Xiying River Basin)

129 **3. Data and methods**

130 **3.1 Sample collection**

131 In this study, soil water and precipitation samples were collected from four
 132 vegetation zones in the Xiying River basin from April to October in 2017 (plant
 133 growing season). In 2017, the precipitation in the alpine meadow, coniferous forest,
 134 mountain grassland and deciduous forest were 595.1 mm, 431.9 mm, 363.5 mm and

135 262.5 mm, respectively. The average daily temperature in the alpine meadow,
 136 coniferous forest, mountain grassland and deciduous forest were -0.19°C, 3.34°C,
 137 6.6°C and 7.9°C, respectively (Table 1).

138 Collection of soil samples: Soil samples were collected once a month at depths
 139 of 0-10, 10-20, 20-30, 30-40, 40-50, 50-60, 60-70, 70-80, 80-90, and 90-100 cm from
 140 the soil layers in the four vegetation zones. Three duplicate samples were collected for
 141 each soil layer. We placed the collected soil sample into a 50 mL glass bottle, sealed
 142 the bottle mouth with Parafilm and marked the sampling date. We froze the sample for
 143 storage until experimental analysis. Each sample was collected separately in an
 144 aluminum box.

145 Collection of precipitation samples: The precipitation samples were collected by
 146 a plastic funnel bottle device. After each precipitation event, the collected
 147 precipitation samples were immediately transferred to an 80 mL high-density
 148 polyethylene bottle, and the bottle mouth of the samples was sealed with Parafilm;
 149 these samples were also frozen and stored until experimental analysis.

150 Meteorological data: During the sampling period, the local meteorological data
 151 were obtained and recorded by automatic weather stations (Watchdog 2000 series
 152 weather stations) set up near the sample plot.

153 **Table 1** Basic data of each Vegetation zone from April to October 2017 (*Long*-Longitude,
 154 *Lat*-Latitude, *Alt*-Altitude, *T*-Air Temperature (daily mean temperature), *P*-Precipitation (total
 155 precipitation during the observation period), *h*-Relative Humidity (daily mean relative humidity))

Vegetation zone	Geographical parameters			Meteorological parameters			Number of samples	
	<i>Long</i> (°E)	<i>Lat</i> (°N)	<i>Alt</i> (m)	<i>T</i> (°C)	<i>P</i> (mm)	<i>h</i> (%)	Precipitation	Soil
Alpine Meadow	101°51'16"	37°33'28"	3637	-0.19	595.1	69.2	72	47
Coniferous Forest	101°53'23"	37°41'50"	2721	3.34	431.9	66.6	42	41
Mountain Grassland	102°00'25"	37°50'23"	2390	6.6	363.5	60.4	37	54
Deciduous Forest	102°10'56"	37°53'27"	2097	7.9	262.5	59.8	40	53

156 **3.2 Sample determination**

157 The analysis of $\delta^2\text{H}$ and $\delta^{18}\text{O}$ values of all the above water samples was
 158 completed using a liquid water isotope analyzer (DLT-100, Los Gatos Research, USA)
 159 in the stable isotope laboratory of Northwest Normal University. Before analyzing the
 160 isotope values of soil water, the soil water was extracted from the collected soil
 161 samples by a low-temperature vacuum condensation system (LI-2100, LICA United
 162 Technology Limited, China). Both the water and isotope standard samples were
 163 injected 6 times during the analysis. To avoid the “memory effect” of isotope analysis,
 164 we discarded the first two injection values and used the average value of the last four
 165 injections as the final result (Penna et al., 2012; Qu et al., 2020). The analysis results
 166 were relative to VSMOW (Vienna Standard Mean Ocean Water):

$$\delta = \left(\frac{R_{\text{sample}}}{R_{\text{standard}}} - 1 \right) \times 1000\text{‰} \quad (1)$$

167 where R_{sample} is the ratio of $^{18}\text{O}/^{16}\text{O}$ or $^2\text{H}/^1\text{H}$ in the sample and R_{standard} is the ratio of
 168 $^{18}\text{O}/^{16}\text{O}$ or $^2\text{H}/^1\text{H}$ in the VSMOW. The test error of the $\delta^2\text{H}$ value does not exceed
 169 $\pm 0.6\text{‰}$, and the test error of the $\delta^{18}\text{O}$ value does not exceed $\pm 0.2\text{‰}$.

170 3.3 Analysis method

171 3.3.1 Lc-excess

172 The linear relationship between $\delta^2\text{H}$ and $\delta^{18}\text{O}$ in precipitation and soil water is
 173 defined as the LMWL (local meteoric water line) and SWL (soil waterline),
 174 respectively, which are of great significance for studying the evaporative fractionation
 175 of stable isotopes during the water cycle. We further calculated the line-conditioned
 176 excess for each soil water and precipitation sample. The lc-excess in different water
 177 bodies can characterize the evaporation index of different water bodies relative to the
 178 local precipitation (Landwehr and Coplen, 2006).

$$\text{lc-excess} = \delta^2\text{H} - a \times \delta^{18}\text{O} - b \quad (2)$$

179 where a and b are the slope and intercept of the LMWL, respectively, and $\delta^2\text{H}$ and
 180 $\delta^{18}\text{O}$ are the isotopic values of hydrogen and oxygen in the sample. The physical
 181 meaning of lc-excess is expressed as the degree of deviation of the isotope value in
 182 the sample from the LMWL, indicating the nonequilibrium dynamic fractionation

183 process caused by evaporation. Generally, the change in lc-excess in local
 184 precipitation is mainly affected by different water vapor sources, and the annual
 185 average is 0. Since the stable isotopes in soil water are enriched by evaporation, the
 186 average lc-excess is usually negative (Landwehr et al., 2014; Sprenger et al., 2017).

187 3.3.2 Potential evapotranspiration

188 The potential evapotranspiration was calculated based on the Penman-Monteath
 189 equation (Allen, 1998):

$$\text{PET} = \frac{0.408\Delta(R_n - G) + \gamma \frac{900}{T + 273} u^2 (e_s - e_a)}{\Delta + \gamma(1 + 0.34u^2)} \quad (3)$$

190 where PET is the daily potential evapotranspiration (mm day⁻¹), R_n is the net radiation
 191 (MJ m² day⁻¹), G is the soil heat flux density (MJ m² day⁻¹), γ is the psychrometric
 192 constant (kPa°C⁻¹), u_2 is the wind speed at 2 m height (m s⁻¹), T is the mean daily air
 193 temperature at 2 m height (°C), Δ is the slope of the vapor pressure curve (kPa°C⁻¹), e_a
 194 is the actual vapor pressure (kPa) and e_s is the saturated vapor pressure (kPa). These
 195 data come from nearby weather stations.

196 3.3.3 Soil water storage

197 Soil water storage is the thickness of the water layer formed by all the water in a
 198 certain soil layer (Milly, 1994) and is expressed by the following formula:

$$S = R \times W \times H \times 10 \quad (4)$$

199 where S is the soil water storage in a certain thickness layer (mm), R is the soil bulk
 200 density (g cm⁻³), and H is the soil thickness (cm). W is the gravimetric water content,
 201 which is expressed by the following formula:

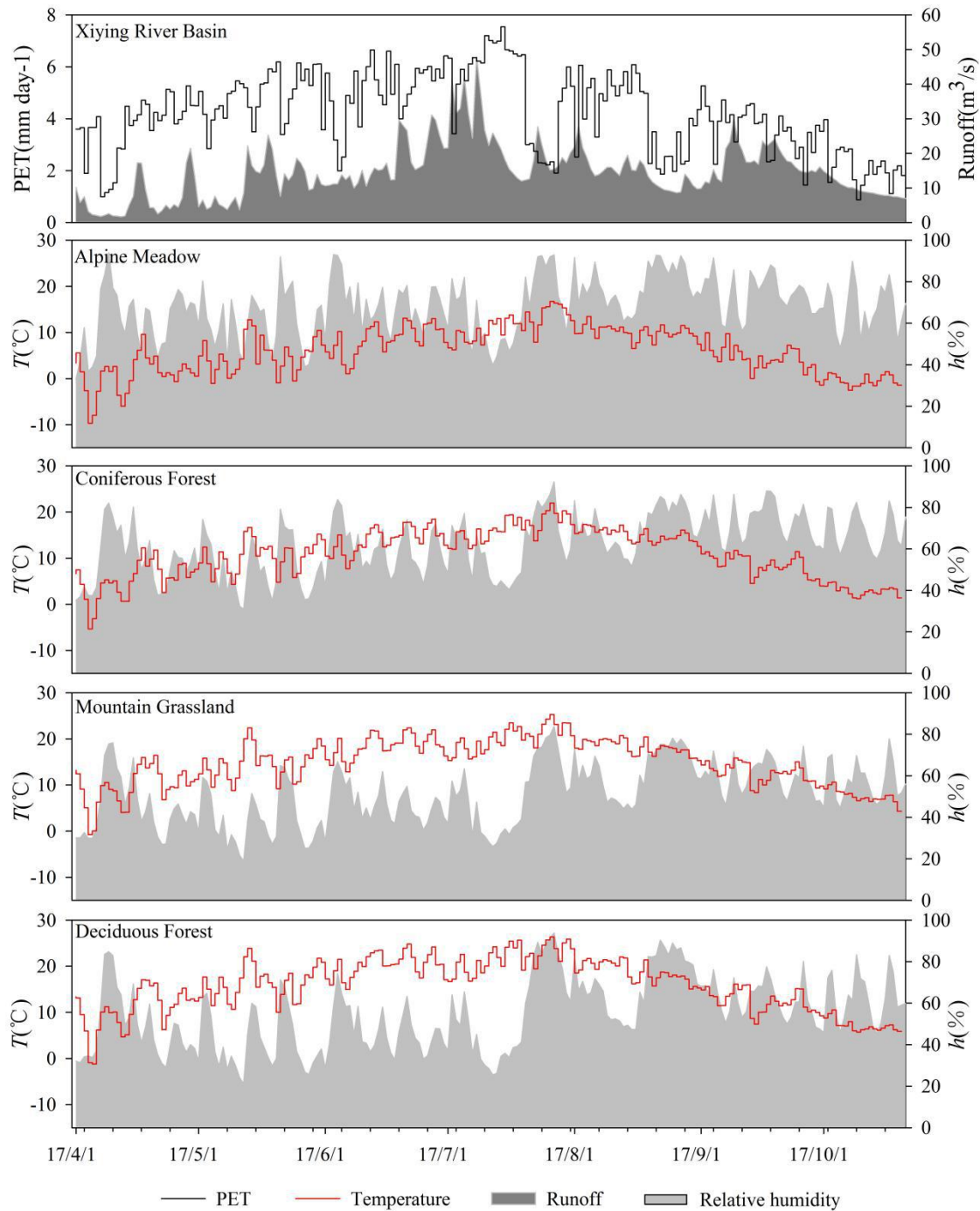
$$W = \frac{M_1 - M_2}{M_2} \times 100\% \quad (5)$$

202 in the formula, M_1 is the gravimetric value of wet soil (g), and M_2 is the gravimetric
 203 value of dry soil (g).

204 4. Results and analysis

205 4.1 Hydrological climate

206 PET and runoff are important indicators that reflect the dry-wet conditions of
207 river basins. During the study period (April-October 2017), in the Xiyang River Basin,
208 the potential evapotranspiration was 872.8 mm, the daily evapotranspiration ranged
209 from 7.5 mm (July 14) to 0.9 mm (October 9), showing a fluctuating trend around
210 July, and the PET value in April-July was higher than that in August-October. The
211 input of summer precipitation and ice/snow meltwater increased runoff, resulting in a
212 trend similar to PET. During the observation period, the total runoff was 3.1×10^9 m,
213 accounting for 89% of the annual runoff. The variation range of the daily runoff was
214 286848 m^3 (April 17) to 6125760 m^3 (July 13). The basin before July was drier than
215 that after July (Fig. 2).



216

217 **Fig. 2** Climatic and hydrological conditions of Xiying River basin

218 To explore the differences in the natural environment in different vegetation
 219 zones, air temperature, atmospheric humidity, and precipitation were used to indicate
 220 each research site's temperature and moisture conditions. The hilltop is a typical
 221 alpine meadow zone, with a daily average temperature of 6.1°C, ranging from -9.7°C
 222 (April 5) to 16.8°C (July 27). The daily average humidity was 68.2%, with little

223 difference in different periods. During the observation period, there were 72
224 precipitation events in the alpine meadow zone, and the total precipitation was 534.3
225 mm, which was relatively evenly distributed each month. In the coniferous forest zone,
226 the daily average temperature during the study period was 10.9°C, ranging from
227 -5.4°C (April 5) to 22.0°C (July 27). The daily average humidity was 62.5%, and the
228 precipitation was 400.6 mm, mainly concentrated from early August to late September.
229 Close to the foothills is the mountain grassland zone, with a daily average temperature
230 of 14.9°C, ranging from -0.7°C (April 5) to 25.3°C (July 27). The average daily
231 humidity was 51.1%, and the precipitation of the vegetation zone during the
232 observation period was 327.2 mm, mainly from late July to mid-August. During the
233 observation period, the daily average temperature in the deciduous forest zone was
234 15.8°C, ranging from -1.2°C (April 6) to 26.3°C (July 27). The daily average
235 humidity was 54.7%, and the total precipitation was 250.6 mm, which was
236 concentrated in the month from late July to late August. The temperature of the
237 studied regions were ordered as follows: AM (alpine meadow) < CF (coniferous
238 forest) < MG (mountain grassland) < DF (deciduous forest). The humidities of the
239 studied regions were ordered as follows: AM > CF > MG > DF (Fig. 2).

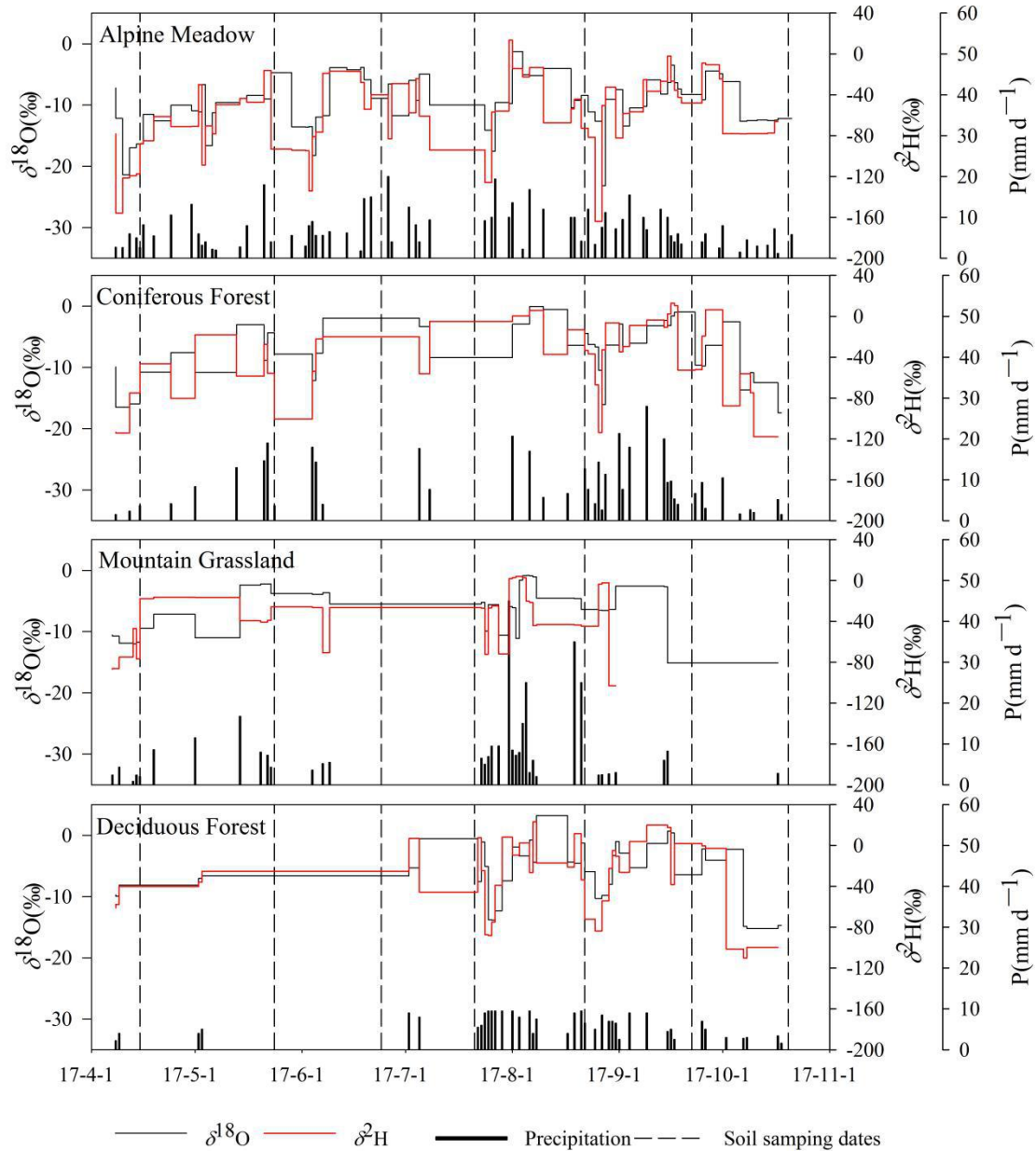
240 **4.2 Temporal variation in water stable isotopes in different vegetation zones**

241 Influenced by different water sources and complex weather conditions in the
242 precipitation process, the isotopic compositions of precipitation in the four vegetation
243 zones were different during the study period. The mean values of $\delta^2\text{H}$ and $\delta^{18}\text{O}$ in the
244 alpine meadow zone (number of samples: 72) were $-73.1\text{‰}\pm 36.3\text{‰}$ ($-163.9\sim 13.7\text{‰}$)
245 and $-10.0\text{‰}\pm 4.3\text{‰}$ ($-23.1\sim -1.3\text{‰}$), respectively. The average $\delta^2\text{H}$ and $\delta^{18}\text{O}$ values of
246 the coniferous forest zone (number of samples: 42) were $-42.0\text{‰}\pm 37.2\text{‰}$
247 ($-117.8\sim 13.0\text{‰}$) and $-7.1\text{‰}\pm 4.7\text{‰}$ ($-17.4\sim -0.1\text{‰}$), respectively. The average $\delta^2\text{H}$ and
248 $\delta^{18}\text{O}$ values of the mountain grassland zone (number of samples: 37) were
249 $-37.4\text{‰}\pm 30.5\text{‰}$ ($-103.1\sim 4.2\text{‰}$) and $-5.9\text{‰}\pm 3.9\text{‰}$ ($-15.1\sim -0.9\text{‰}$), respectively. The
250 average $\delta^2\text{H}$ and $\delta^{18}\text{O}$ values of the deciduous forest zone (number of samples: 40)
251 were $-31.8\text{‰}\pm 42.8\text{‰}$ ($-110.2\sim 23.2\text{‰}$) and $-5.8\text{‰}\pm 5.5\text{‰}$ ($-15.2\sim 3.2\text{‰}$), respectively
252 (Table 2). The maximum isotopic values of the four vegetation zones appeared on

253 August 4 (AM: 13.7‰, $\delta^2\text{H}$; -1.3‰, $\delta^{18}\text{O}$), August 10 (CF: 13.0‰, $\delta^2\text{H}$; -0.1‰,
 254 $\delta^{18}\text{O}$), August 7 (MG: 4.2‰, $\delta^2\text{H}$; -0.9‰, $\delta^{18}\text{O}$) and August 13 (DF: 23.2‰, $\delta^2\text{H}$;
 255 3.2‰, $\delta^{18}\text{O}$). The highest temperature in each vegetation zone appeared on July 27.
 256 The high temperature caused the precipitation to undergo strong below-cloud
 257 evaporation during the fall, leading to the enrichment of isotopes. In addition, the
 258 atmospheric precipitation isotopes of the four vegetation zones had similar temporal
 259 variations: from April to August, the fluctuations in $\delta^2\text{H}$ and $\delta^{18}\text{O}$ increased, reached
 260 the maximum in mid-August, and then gradually decreased (Fig. 3).

261 **Table 2** General characteristics of precipitation $\delta^2\text{H}$ and $\delta^{18}\text{O}$ in different vegetation areas
 262 from April to October 2017

Vegetation zone	$\delta^2\text{H}/\text{‰}$				$\delta^{18}\text{O}/\text{‰}$			
	Max	Min	mean	SD	Max	Min	mean	SD
AM	13.7	-163.9	-73.1	36.3	-1.3	-23.1	-10.0	4.3
CF	13.0	-117.8	-42.0	37.2	-0.1	-17.4	-7.1	4.7
MG	4.2	-103.1	-37.4	30.5	-0.9	-15.1	-5.9	3.9
DF	23.2	-110.2	-31.8	42.8	3.2	-15.2	-5.8	5.5



263

264 **Fig. 3** Time series of rainfall and isotope characteristics in different vegetation
 265 zones in Xiying River Basin, with dotted lines indicating the date of soil water
 266 sampling

267 The monthly variation in soil water isotopes records the signal of precipitation
 268 input and evaporation. The low-temperature environment and abundant precipitation
 269 events in the alpine meadow make the monthly average $\delta^2\text{H}$ and $\delta^{18}\text{O}$ of soil water
 270 more depleted than other vegetation zones ($-69.4\sim-51.6\text{‰}$, $\delta^2\text{H}$; $-7.5\sim-10.3\text{‰}$, $\delta^{18}\text{O}$).
 271 Despite this, the SWlc-excess of most samples at this station was still negative, and
 272 there were different degrees of evaporation in the process of precipitation penetrating

273 the soil and mixing with original pore water, among which evaporation fractionation
274 was stronger in July (-11.9‰ lc-excess) and October (-14.5‰ lc-excess). The soil
275 water isotopes of the coniferous forest gradually changed seasonally. From April to
276 July, precipitation was scarce, the temperature rose, and the isotopes of soil water
277 were gradually enriched on the surface (-52.7~-29.5‰, $\delta^2\text{H}$; -7.0~-2.1‰, $\delta^2\text{H}$),
278 reaching the peak value of the observation period in July (-29.5‰, $\delta^2\text{H}$; -2.1‰, $\delta^{18}\text{O}$),
279 and continuous rainfall input from late July to mid-August resulted in soil water
280 isotope depletion (-57.0‰, $\delta^2\text{H}$; -8.1‰, $\delta^{18}\text{O}$). SWlc-excess was an obvious
281 fractionation signal opposite to the trend of isotope change, reaching the lowest value
282 (-26.3‰) in the sampling period in July, and the change in air temperature and
283 precipitation controlled the evaporation intensity. From April to July, the isotopic
284 value of surface soil water in the mountain grassland was higher ($\delta^{18}\text{O}$ was greater
285 than zero), and SWlc-excess was lower than -30‰. During this period, the
286 evaporation and fractionation of shallow soil water were intense. Similar to in the
287 coniferous forest, in the mountain grassland, the input of heavy precipitation from late
288 July to mid-August led to the depletion of soil water isotopes. There was only
289 sporadic rainfall in the deciduous forest from April to July, and the soil water isotopes
290 were gradually enriched on the surface (-46.1~-18.2‰, $\delta^2\text{H}$; -4.7~-0.2‰, $\delta^2\text{H}$),
291 reached a peak in June when there was no rainfall event (-18.2‰, $\delta^2\text{H}$; 0.2‰, $\delta^{18}\text{O}$),
292 and then became depleted (-53.2‰, $\delta^2\text{H}$; -5.2‰, $\delta^{18}\text{O}$). In addition, due to the
293 influence of the Xiyang Reservoir and vegetation coverage, the isotopic enrichment
294 degree of soil water in this vegetation zone was lower than that in the mountain
295 grassland. As the most intuitive form of water change, the gravimetric water content
296 was always at a low value in July (AM: 21.0%; CF: 14.8%; MG: 11.9%; DF: 14.9%),
297 when the evaporation was the strongest, and it was most obvious in shallow soil
298 (Table 3) (Fig. 4).

299

300

301

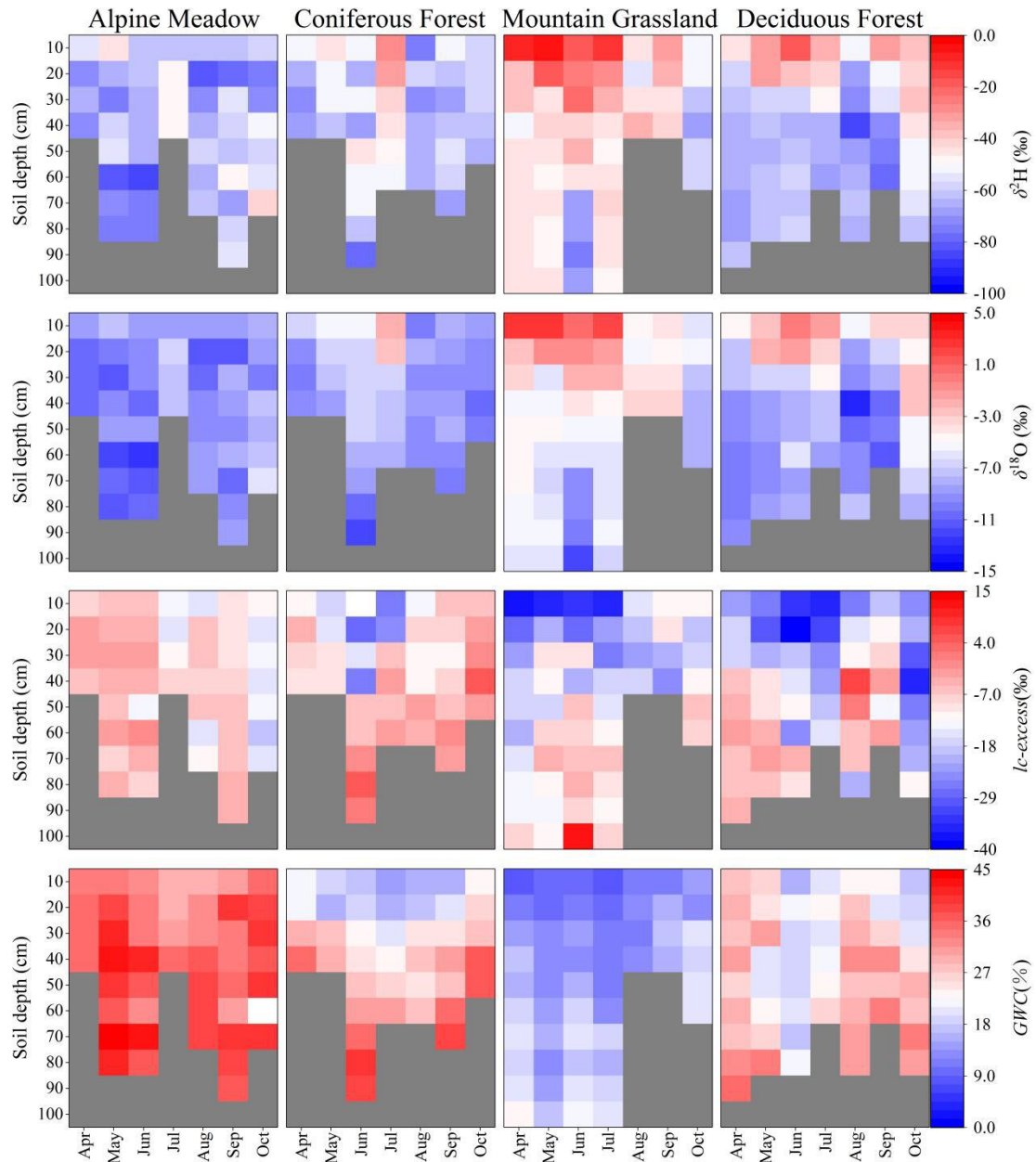
302

Table 3 General characteristics of soil water $\delta^2\text{H}$, $\delta^{18}\text{O}$, lc-excess and GWC in different

303

vegetation areas from April to October 2017

Month	Vegetation zone	$\delta^2\text{H}/\text{‰}$			$\delta^{18}\text{O}/\text{‰}$			lc-excess/ ‰			GWC/ ‰		
		Max	Min	Mean	Max	Min	Mean	Max	Min	Mean	Max	Min	Mean
4	AM	-55.2	-70.7	-65.6	-8.5	-10.8	-10.1	-2.7	-7.1	-4.7	25.9	23.0.0.	24.7
	CF	-52.7	-72.2	-63.9	-7.0	-9.9	-8.9	-4.0	-12.0	-8.4	27.6	14.9	20.0
	MG	-7.32	-50.6	-41.0	2.8	-5.8	-3.9	-8.8	-36.8	-19.4	21.7	6.5	14.7
	DF	-46.1	-69.4	-62.1	-4.7	-9.9	-8.5	-2.5	-23.2	-9.7	27.7	19.4	21.8
5	AM	-46.1	-76.5	-66.4	-7.4	-12.2	-10.1	-2.6	-7.7	-4.9	32.6	23.2	28.9
	CF	-45.8	-61.9	-53.5	-5.3	-8.4	-7.0	-9.3	-17.7	-13.0	22.6	9.0	16.1
	MG	-6.7	-47.3	-39.2	2.9	-6.5	-4.3	-4.5	-36.2	-14.4	15.7	7.6	11.2
	DF	-30.8	-63.5	-53.8	-1.9	-9.4	-6.9	-3.2	-30.1	-13.6	26.0	11.7	17.7
6	AM	-62.5	-83.9	-69.4	-8.9	-12.6	-10.3	-1.5	-8.4	-5.8	33.3	21.9	26.0
	CF	-45.8	-78.4	-58.7	-5.1	-12.0	-7.8	5.5	-26.6	-8.5	32.1	10.0	21.3
	MG	-19.7	-74.9	-46.9	0.8	-11.8	-5.8	13.0	-33.7	-11.0	19.3	7.5	14.2
	DF	-18.2	-64.9	-51.7	0.2	-9.0	-5.9	-4.6	-38.2	-19.4	13.5	8.4	11.1
7	AM	-47.3	-60.1	-51.6	-6.9	-8.4	-7.5	-8.8	-14.8	-11.9	25.4	19.0	21.0
	CF	-29.5	-51.4	-41.6	-2.1	-7.9	-5.6	-2.6	-26.3	-11.2	24.3	7.2	14.8
	MG	-10.6	-48.4	-39.2	2.3	-6.4	-4.1	-5.8	-35.8	-16.1	18.7	6.3	11.9
	DF	-35.1	-69.0	-54.1	-1.7	-8.7	-5.5	-14.8	-35.3	-24.5	18.2	11.8	14.4
8	AM	-58.5	-80.3	-66.6	-8.4	-11.6	-9.6	-6.1	-15.4	-9.7	28.1	19.5	25.1
	CF	-57.0	-75.5	-66.4	-8.1	-9.8	-9.2	-2.5	-13.1	-8.3	21.4	8.7	16.3
	MG	-34.2	-53.8	-44.0	-3.2	-5.5	-4.4	-14.7	-22.6	-18.7	11.3	9.5	10.4
	DF	-53.2	-84.3	-67.6	-5.2	-13.5	-9.2	6.8	-26.1	-9.6	23.6	14.7	20.6
9	AM	-48.0	-79.2	-61.0	-7.8	-11.1	-9.2	-4.3	-10.4	-7.2	29.9	20.3	25.3
	CF	-52.5	-67.7	-60.7	-7.8	-10.1	-8.8	-0.1	-11.3	-6.0	31.3	9.3	20.5
	MG	-32.3	-45.3	-38.8	-3.5	-4.4	-4.0	-9.1	-23.8	-16.5	15.3	9.1	13.0
	DF	-30.5	-77.0	-59.8	-3.1	-11.4	-8.2	-1.8	-19.3	-9.3	25.8	14.7	19.1
10	AM	-42.4	-73.5	-58.9	-6.1	-9.8	-7.9	-12.2	-18.2	-14.5	36.2	25.4	29.5
	CF	-59.1	-66.3	-61.7	-8.8	-10.5	-9.5	5.1	-5.3	-1.5	30.0	16.8	23.1
	MG	-50.3	-66.7	-58.3	-5.6	-8.3	-7.1	-5.5	-18.4	-11.9	18.3	11.4	15.8
	DF	-38.0	-61.8	-48.3	-2.7	-8.2	-4.9	-11.9	-34.8	-23.9	25.5	8.9	17.2



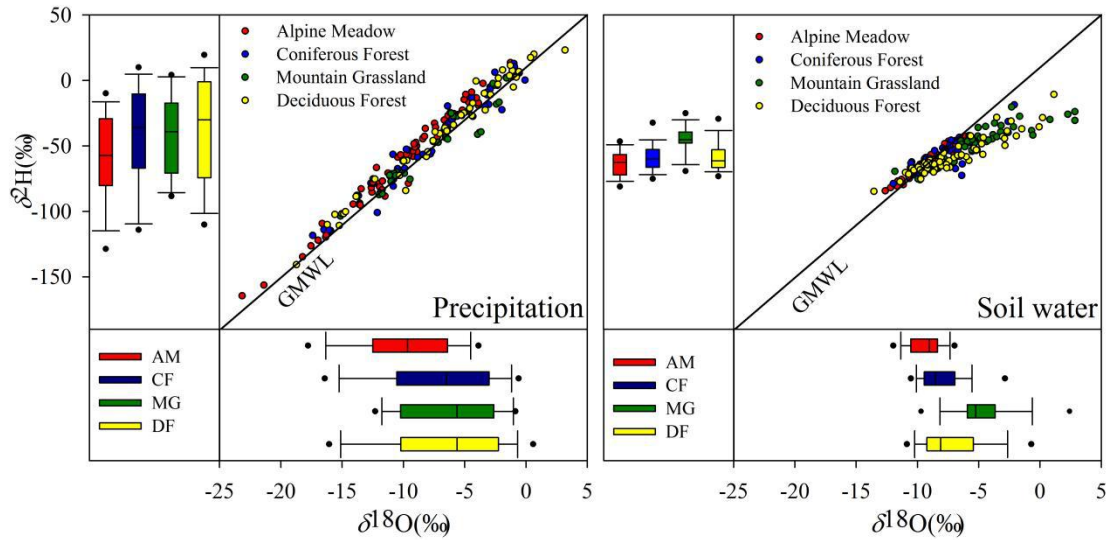
304

305 **Fig. 4** Heat map of the soil depth profile of $\delta^2\text{H}$, $\delta^{18}\text{O}$, lc-excess and GWC in
 306 different vegetation zones, and the layer lacking measurement is indicated by the
 307 grey color

308 **4.3 Spatial variation in water stable isotopes in different vegetation zones**

309 Isotope data of precipitation and soil water obtained from different vegetation
 310 zones are shown in dual-isotope space in Fig. 5. At the alpine meadow observation
 311 station, the slope (8.4) and intercept (23) of the LMWL were higher than those of the
 312 GMWL. The slope of the LMWL in the other three vegetation zones was lower than
 313 that of the GMWL and gradually decreased with decreasing altitude. With the

314 decrease in altitude, the slope of the SWL in all vegetation zones except for the
 315 deciduous forest SWL decreased (AM: 6.4; CF: 4.7; MG: 3.4; DF: 4.1), indicating
 316 that the evaporation of soil moisture increased. On the one hand, the vegetation
 317 coverage of the deciduous forest site was higher. On the other hand, the Xiying
 318 Reservoir enhanced the regional air humidity and decreased the local water vapor
 319 circulation driving force.

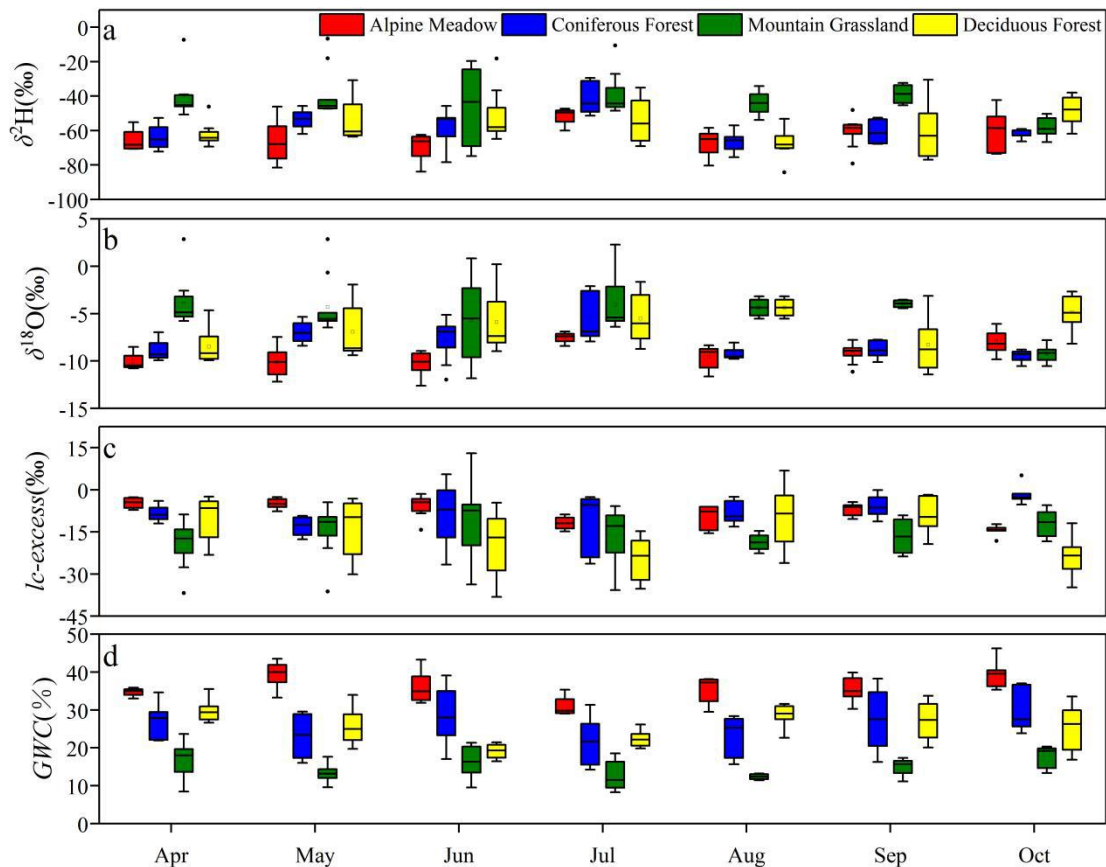


320

321 **Fig. 5** Dual-isotope space of precipitation (left) and soil water (right) isotope data of
 322 four vegetation zones. In the box plots, the box represents the 25%-75% percentile,
 323 the line in the box represents the median (50th percentile), the required line
 324 indicates 90th and 10th percentile, and the point indicates the 95th and 5th
 325 percentile.

326 During the study period, compared with that in other vegetation belts, the surface
 327 isotopic value of the soil water in the mountain grassland was relatively enriched
 328 (-24.3‰, $\delta^2\text{H}$; -0.8‰, $\delta^{18}\text{O}$), the lc-excess was smaller and deeper into the middle
 329 and lower soil layers (-25.8‰), and the gravimetric water content was relatively low
 330 (8.4%). Due to the difference in vegetation types and the influence of reservoirs, this
 331 change did not have an obvious elevation effect. Although the elevation was low, the
 332 soil water of the deciduous forest had more depleted isotopic characteristics and
 333 higher soil moisture than those of the mountain grassland in most samples. Soil
 334 profiles obtained from different vegetation zones can reflect the evaporation signals of

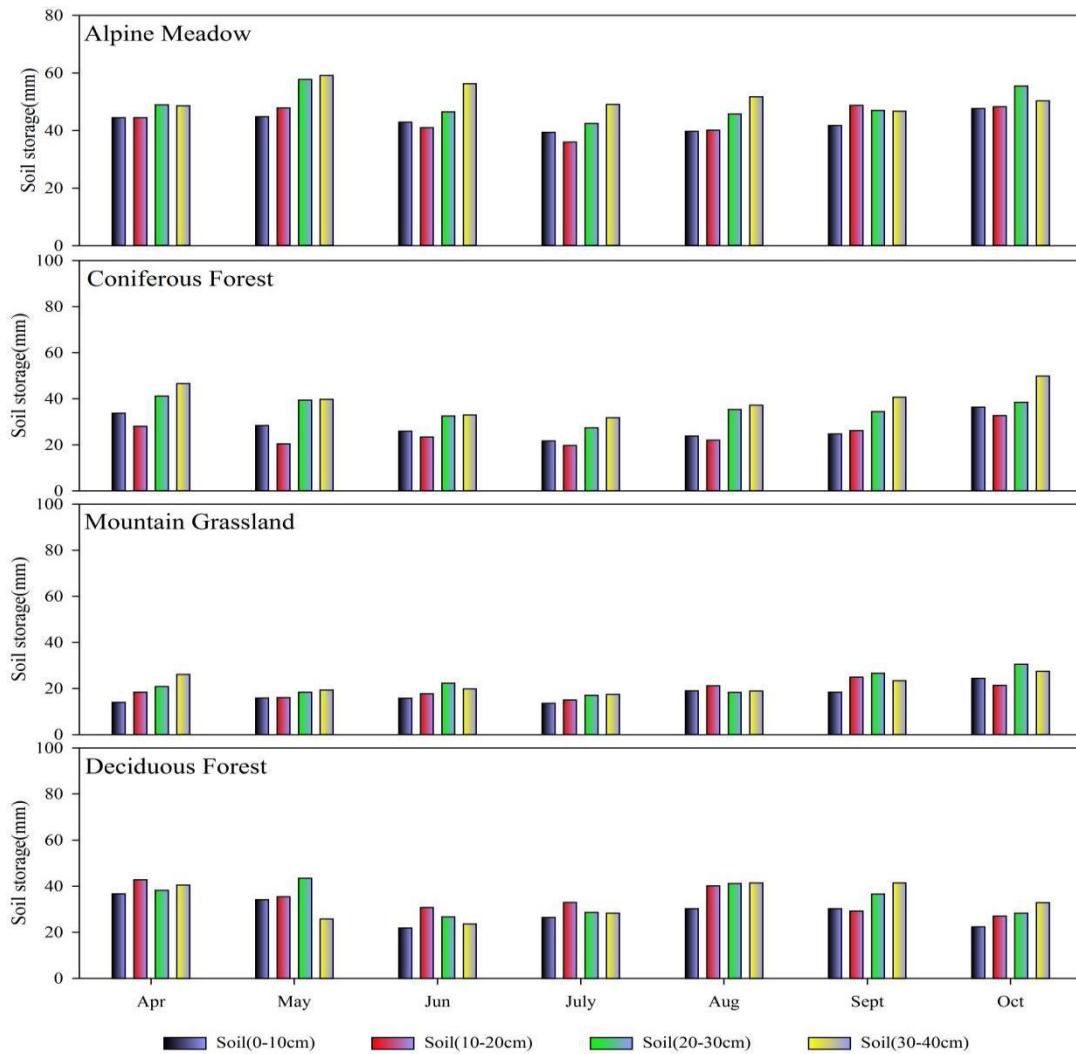
335 water. The low-temperature natural environment made alpine meadow soil less
 336 affected by evaporation ($lc\text{-excess} > -20\%$), and the gravimetric water content was
 337 high (gravimetric water content $> 20\%$) during the whole study period. The surface
 338 soil water of the coniferous forest was easily affected by climate and had a higher
 339 isotopic composition (-29.5% , δ^2H ; -2.1% , $\delta^{18}O$) and lower $lc\text{-excess}$ (-26.3%).
 340 Due to evaporation, soil water isotopes in the mountain grassland and deciduous
 341 forest areas were enriched in the surface soil layer. In particular, in the mountain
 342 grassland, the average values of δ^2H and $\delta^{18}O$ in the 0-10 cm soil layer were as high
 343 as -24.4% and -1.2% , respectively, and $SWlc\text{-excess}$ was lower than -25% , even
 344 close to -40% in some samples. In this case, the evaporation signals can easily
 345 penetrate the deep soil, making the gravimetric water content values at all the
 346 sampling sites lower than 20% (Fig. 4; Fig. 6).



347
 348 **Fig. 6** The variation of δ^2H , $\delta^{18}O$, $lc\text{-excess}$ and GWC in different vegetation zones
 349 in each sampling

350 **4.4 Variations in the water storage capacity of the 0-40 cm soil layer in different**
 351 **vegetation areas**

352 This study used soil water to calculate the water storage of the 0-40 cm soil layer
353 in the four vegetation zones during the observation period (Fig 7). The water storage
354 capacity of the alpine meadow gradually decreased from April to July (209.7~167.2
355 mm), and the water storage capacity increased after July (167.2~201.8 mm). The
356 monthly average water storage capacity was the lowest at 0-10 cm (43.0 mm) and the
357 highest at 30-40 cm (51.7 mm). The water storage capacity of the coniferous forest
358 gradually decreased from April to July (150.1~101.2 mm), and the water storage
359 capacity increased after July (101.2~160.0 mm). The monthly average water storage
360 capacity was the lowest at 0-10 cm (28.0 mm) and the highest at 30-40 cm (40.0 mm).
361 The water storage capacity of the mountain grassland gradually decreased from April
362 to July (80.3~64.0 mm), and the water storage capacity increased after July
363 (64.0~104.6 mm). The monthly average water storage capacity was the lowest at 0-10
364 cm (17.5 mm) and the highest at 20-30 cm (22.0 mm). The water storage capacity of
365 the deciduous forest gradually decreased from April to June (159.3~104.0 mm), the
366 water storage capacity increased from June to August (104.0~154.0 mm), and there
367 was a decrease from August to October (154.0~111.8 mm). The monthly average
368 water storage capacity was the lowest at 0-10 cm (29.1 mm) and the highest at 20-30
369 cm (35.0 mm). In general, the soil water storage capacity of the 0-10 cm soil layer
370 was less than that of the other soil layers. The order of the water storage capacity of
371 the 0-40 cm soil layer in the four vegetation zones is alpine meadow (46.9 mm) >
372 deciduous forest (33.0 mm) > coniferous forest (32.1 mm) > mountain grassland (20.3
373 mm).



374

375 **Fig. 7** Monthly variation of soil water storage in 0-40cm soil layer of different
 376 vegetation zones

377 5. Discussion

378 5.1 Evaporation of soil moisture in different vegetation zones

379 In the arid river source area, the replenishment of soil moisture mainly comes
 380 from precipitation. The slope of the regional atmospheric precipitation line can reflect
 381 the strength of local evaporation. Due to a low atmospheric temperature, low cloud
 382 base height, and low air-saturated water vapor loss, the alpine meadow zone was
 383 weakly affected by secondary evaporation during precipitation. There, the slope of the
 384 LMWL (8.4) was even higher than that of the GMWL (Hughes and Crawford, 2012).
 385 As the altitude decreased, the secondary evaporation under clouds strengthened, and

386 the slope of the LMWL of each vegetation zone decreased (Pang et al., 2011). The
387 slope of SWL can indicate the strength of soil moisture evaporation in each vegetation
388 zone, the evaporation intensity results of the four vegetation zones followed the order
389 of mountain grassland ($SWL_{slop}: 3.4$) > deciduous forest ($SWL_{slop}: 4.1$) > coniferous
390 forest ($SWL_{slop}: 4.7$) > alpine meadow ($SWL_{slop}: 6.4$) (Fig 5). The dynamic changes in
391 lc-excess of soil profiles in different vegetation areas reflect the process of soil water
392 evaporation caused by drought during the study period. The monthly average value of
393 SWlc-excess in the alpine meadow zone was less than 0, and the minimum value was
394 -11.9‰ (July). Although the vegetation belt was subject to different degrees of
395 evaporation each month, it was less affected by drought, and it was difficult for
396 evaporation to penetrate into the middle and lower soil layers. The SWlc-excess of the
397 coniferous forest belt was greater than that of the alpine meadow from April to June.
398 The evaporation was the strongest in July (-11.2‰ lc-excess). Similar to in the alpine
399 meadow, in the coniferous forest belt, evaporation mainly occurred in the topsoil. The
400 vegetation coverage of the mountain grassland zone was low, and the arid
401 environment made the isotopes of the surface soil produce strong evaporation signals
402 (lc-excess was close to -40‰). In most samples, the SWlc-excess of the 60-80 cm soil
403 layer was negative. The evaporation signal shifted to the lower layer of the soil
404 (Barnes and Allison, 1988; Zimmermann et al., 1966). Similar evaporation signals
405 have been found in the Mediterranean and arid climate regions (McCutcheon et al.,
406 2017; Sprenger et al., 2016). Evaporation signals exist in only the surface soil in
407 humid areas, and there is no difference between lc-excess and 0 in the soil layer below
408 20 cm (Sprenger et al., 2017). The monthly surface soil evaporation of deciduous
409 forest was less than that of mountain grassland from April to June, and it was greater
410 than that of mountain grassland after July, mainly due to the influence of the
411 vegetation and reservoirs. There were commonalities in the soil moisture changes in
412 different vegetation zones characterized by more enriched isotopes, stronger
413 evaporation signals, and lower moisture content in the shallow soil. With increasing
414 soil depth, the isotope gradually became depleted, and the evaporation signal was
415 gradually weakened until it disappeared. The evolution of the investigated isotopes,

416 lc-excess, and gravimetric water content in the unsaturated soil showed differences
417 among different vegetation zones. From a high altitude to a low altitude, the isotopic
418 value of the surface gradually increased, and the evaporation signal increased (Fig 4;
419 Fig 6).

420 **5.2 Memory effects of precipitation input, mixing and rewetting**

421 The changes in soil water isotopes and soil moisture can evaluate the input,
422 mixing, and rewetting precipitation process in different vegetation areas. The main
423 methods of precipitation input are plug flow and preferential flow. Plug flow is the
424 complete mixing of water through the soil matrix with shallow free water. Under the
425 action of plug flow, precipitation infiltrates along the hydraulic gradient, pushing the
426 original soil water downward. Preferential flow means that precipitation uses soil
427 macropores to quickly penetrate shallow soil to form deep leakage (Tang and Feng,
428 2001). After precipitation, the variability of isotope signals at a certain soil depth can
429 identify the seepage method of water (Peralta-Tapia et al., 2015). During the study
430 period, the soils of the alpine meadow and coniferous forest areas were seasonally
431 frozen and thawed year-round, and the difference in the soil isotope profile was small.
432 The soil moisture profile showed a trend of water increasing from top to bottom,
433 indicating the influence of the previous precipitation. The soil was humid, so the
434 replenishment of soil water by precipitation had the characteristics of top-down piston
435 replenishment. Preferential infiltration showed high variability in isotopic signals
436 (Brodersen et al., 2000), and the rainwater in mountain grassland and deciduous forest
437 flowed into the deep soil rapidly through the soil matrix via exposed soil fissures and
438 roots. This resulted in the sudden depletion of soil isotopes at a depth of 60-100 cm.
439 This may be due to the more recent depleted precipitation that quickly reached this
440 depth and the preferential infiltration into the soil. Water movement and mixing in the
441 unsaturated zone can be observed in the spatiotemporal variation in isotopes within 1
442 m of the soil profile, and the alpine meadow and coniferous forest zones underwent
443 considerable rainfall. After a short period of weak evaporation, the soil was rewetted
444 by the next rainfall. In the alpine meadow, the soil moisture remained above 20% each
445 month. The mountain grassland and deciduous forest zones had only sporadic

446 precipitation from mid-May to late July, and the soil moisture evaporated rapidly.
447 With the decrease in air temperature and the occurrence of continuous precipitation
448 after July, the soil was rewetted after two months of drought, and both vegetation
449 zones showed the replacement and mixing of soil water isotopes and precipitation.
450 The results showed that the soil water storage capacity of the alpine grassland was
451 seriously insufficient, reflecting the incomplete rewetting of the soil by precipitation
452 at the end of the study. In addition, low soil water storage capacity will enrich the
453 remaining soil water isotopes (Barnes and Allison, 1988; Zimmermann et al., 1966).
454 We observed the memory effect of soil rewetting caused by precipitation input and the
455 mixing of different vegetation areas during the entire study period. The changes in
456 soil moisture in each vegetation area reflect different climatic and hydrological
457 characteristics (Fig. 4; Fig. 6).

458 **5.3 Influencing factors of soil water storage capacity in arid headwater areas**

459 As the temperature decreased rapidly with increasing height, precipitation and
460 humidity increased to a certain extent, and the vegetation showed a strip-like
461 alternation approximately parallel to the contour line, forming zonal vegetation with
462 obvious differentiation (Yin et al., 2020). The dry-wet conditions of different
463 vegetation zones restricted the soil water storage capacity in the basin. In the process
464 of low-altitude vegetation zone replacement, the precipitation decreased, the
465 temperature rose, the groundwater level dropped, and the soil water storage capacity
466 was weak (Coussement et al., 2018; Kleine et al., 2020). The soil water storage
467 capacity of the alpine meadow zone with low-temperature and rainy weather was
468 higher than that of other vegetation zones (results of the 0-40 cm soil layers from
469 April to October: AM: 187.8 mm; CF: 128.4 mm; MG: 81.2 mm; DF: 132.1 mm).
470 During the study period, the soil water storage capacity (0-40 cm) exceeded 165 mm
471 each month. With the decrease in altitude, the monthly difference in dry-wet
472 conditions in each vegetation zone gradually became obvious. With the increase in
473 temperature in summer, the environment became dry, and the soil water storage
474 capacity weakened (Sprenger et al., 2017). The soil water storage capacity of the
475 coniferous forest zone began to decrease in April, and the water storage capacity of

476 the 0-40 cm layer reached the minimum value (101.2 mm) in July. The variation in
477 temperature and precipitation was the main reason for the monthly difference
478 (Dubber and Werner, 2019). Although there was a certain water storage capacity in
479 the coniferous forest with some transpiration loss, the soil water storage capacity in
480 this vegetation zone was not strong. The water storage capacity of mountain grassland
481 soil was lower than that of other vegetation zones. The continuous dry and warm
482 weather in spring and summer led to the water storage capacity of 0-40 cm soil being
483 lower than that of 100 mm every month. In particular, drought stress leads to
484 insufficient soil moisture, making it difficult to maintain plant demand, resulting in
485 sparse vegetation and large-scale exposed surface soil, which further accelerates
486 surface water loss. The continuous precipitation from the end of July prevented
487 further drought development, and the water input gradually restored the soil water
488 storage capacity (Kleine et al., 2020). The deciduous forest had hydrothermal
489 conditions similar to those of the mountain grassland, but the soil porosity of the
490 forest zone was obviously larger than that of the barren land, and its permeability was
491 higher than that of the barren land. Precipitation infiltrated the ground through roots
492 and turned into groundwater. The forest acted as a reservoir due to its strong water
493 storage and soil conservation capacity (Sprenger et al., 2019). The water storage
494 capacity of the 0-40 cm soil layer in the deciduous forest was higher than 100 mm at
495 each sampling time. In addition, the water content of the 0-40 cm soil layer in each
496 vegetation zone increased with the deepening of the soil layer, and the water storage
497 capacity of the surface soil was weak. The difference in soil properties also led to
498 more water storage in the middle and lower soil layers with higher clay contents
499 (Milly, 1994) (Fig. 7). Climate warming and the spatiotemporal imbalance of water
500 resources have disturbed the ecological-water balance of different vegetation zones in
501 inland river source areas (Liu et al., 2015). Plant growth mainly depends on the water
502 stored in shallow soil layers (Amin et al., 2020). Drought reduces soil water storage
503 and inhibits plant growth (Li et al., 2020). To effectively improve and manage water
504 resources in arid water source areas, exploring the heterogeneity of hydrological

505 processes among different vegetation zones is necessary. This will provide a reference
506 for the formulation of ecological policies.

507 **6. Conclusion**

508 This work provides further insights into the movement and mixing of soil water in
509 different vegetation zones in arid source regions. During the study period, the
510 dynamic changes in Ic-excess in the soil profiles of different vegetation zones
511 reflected the evaporation signals caused by drought. Soil water evaporation in spring
512 and summer, and insufficient precipitation during the drought period, were the main
513 driving forces of isotopic enrichment in the surface soil. The soil water evaporation
514 intensity of the four vegetation zones followed the order of mountain grassland
515 ($SWL_{slop}: 3.4$) > deciduous forest ($SWL_{slop}: 4.1$) > coniferous forest ($SWL_{slop}: 4.7$) >
516 alpine meadow ($SWL_{slop}: 6.4$). In the mountain grassland and deciduous forest zones,
517 drought caused the evaporation signal to penetrate deep into the middle and lower soil
518 layers. The SWIc-excess below 70 cm of the ground surface remained negative. Soil
519 water isotopes and gravimetric water content record the process of soil rewetting
520 caused by precipitation input and mixing. The alpine meadow and coniferous forest
521 zones have many precipitation events. After a short period of weak evaporation, the
522 soil was rewetted by the next precipitation event. There was only sporadic
523 precipitation in the mountain grassland and deciduous forest belt from mid-May to
524 late July. After July, the temperature dropped, and continuous precipitation wet the
525 soil again after two months of drought. The mountain grassland and deciduous forest
526 zones had only sporadic precipitation from mid-May to late July. With the decrease in
527 air temperature and continuous precipitation after July, the soil was rewetted after two
528 months of drought. Moisture and temperature conditions were the key factors that
529 restricted the soil water storage capacity in the different vegetation zones. The water
530 storage capacity of the 0-40 cm soil layer results followed the order of alpine meadow
531 (46.9 mm) > deciduous forest (33.0 mm) > coniferous forest (32.1 mm) > mountain
532 grassland (20.3 mm). The water storage capacity of the surface soil in each vegetation
533 zone was weak, and more water was stored in the middle and lower soil layers with

534 higher clay contents. The research results can be applied to arid and semi-arid alpine
535 regions and can be valuable for latitude and longitude differentiation. This study
536 mainly emphasized the spatiotemporal heterogeneity of soil water evaporation,
537 infiltration, and water storage in different vegetation zones. These results are
538 important for understanding regional hydrological processes and ecological
539 restoration services in environmentally fragile areas.

540 **Acknowledgments**

541 This research was financially supported by the National Natural Science
542 Foundation of China (41661005, 41867030, 41971036). The authors much thank the
543 colleagues in the Northwest Normal University for their help in fieldwork, laboratory
544 analysis, data processing.

545 **Author Contribution statement**

546 Guofeng Zhu and Leilei Yong conceived the idea of the study; Yuanxiao Xu and
547 Qiaozhuo Wan analyzed the data; Zhigang Sun and Leilei Yong were responsible for
548 field sampling; Zhuangxia Zhang participated in the experiment; Lei Wang participated
549 in the drawing; Leilei Yong wrote the paper; Liyuan Sang, Xi Zhao and Yuwei Liu
550 checked and edited language. All authors discussed the results and revised the
551 manuscript.

552 **Additional Information**

553 Competing Interests: The authors declare no competing interests.

554 **References**

- 555 Allen, R. G.: Crop evapotranspiration :guidelines for computing crop water requirements, FAO
556 irrigation and drainage paper, edited, Food and Agriculture Organization of the United Nations,
557 Rome, 300 pp., 1998.
- 558 Amin, A., Zuecco, G., Geris, J., Schwendenmann, L., McDonnell, J. J., Borga, M., and Penna, D.:
559 Depth distribution of soil water sourced by plants at the global scale: A new direct inference
560 approach, *Ecohydrology*, 13, e2177, <https://doi.org/10.1002/eco.2177>, 2020.
- 561 Barnes, C. J., and Allison, G. B.: Tracing of water movement in the unsaturated zone using stable
562 isotopes of hydrogen and oxygen, *J. Hydrol.*, 100, 143-176,
563 [https://doi.org/10.1016/0022-1694\(88\)90184-9](https://doi.org/10.1016/0022-1694(88)90184-9), 1988.
- 564 Brodersen, C., Pohl, S., Lindenlaub, M., Leibundgut, C., and Wilpert, K. V.: Influence of
565 vegetation structure on isotope content of throughfall and soil water, *Hydrol. Process.*, 14,
566 1439-1448,
567 [https://doi.org/10.1002/1099-1085\(20000615\)14:8<1439::AID-HYP985>3.0.CO;2-3](https://doi.org/10.1002/1099-1085(20000615)14:8<1439::AID-HYP985>3.0.CO;2-3), 2000.

568 Brooks, R. J., Barnard, H. R., Coulombe, R., and McDonnell, J. J.: Ecohydrologic separation of
569 water between trees and streams in a Mediterranean climate, *Nat. Geosci.*, 3, 100-104,
570 <https://doi.org/10.1038/ngeo722>, 2010.

571 Coussement, T., Maloteau, S., Pardon, P., Artru, S., Ridley, S., Javaux, M., and Garré, S.: A
572 tree-bordered field as a surrogate for agroforestry in temperate regions: Where does the water
573 go? *Agr. Water Manage.*, 210, 198-207, <https://doi.org/10.1016/j.agwat.2018.06.033>, 2018.

574 Dansgaard, W.: Stable isotopes in precipitation, *Tellus*, 16, 436-468,
575 <https://doi.org/10.3402/tellusa.v16i4.8993>, 1964.

576 Dubbert, M., and Werner, C.: Water fluxes mediated by vegetation: emerging isotopic insights at
577 the soil and atmosphere interfaces, *New Phytologist*, 221, 1754-1763,
578 <https://doi.org/10.1111/nph.15547>, 2019.

579 Duvert, C., Stewart, M. K., Cendón, D. I., and Raiber, M.: Time series of tritium, stable isotopes
580 and chloride reveal short-term variations in groundwater contribution to a stream, *Hydrol. Earth
581 Syst. Sci.*, 20, 257-277, <https://doi.org/10.5194/hess-20-257-2016>, 2016.

582 Ferretti, D. F., Pendall, E., Morgan, J. A., Nelson, J. A., LeCain, D., and Mosier, A. R.:
583 Partitioning evapotranspiration fluxes from a Colorado grassland using stable isotopes:
584 Seasonal variations and ecosystem implications of elevated atmospheric CO₂, *Plant Soil*, 254,
585 291-303, <https://doi.org/10.1023/A:1025511618571>, 2003.

586 Gibson, J. J., Holmes, T., Stadnyk, T. A., Birks, S. J., Eby, P., and Pietroniro, A.: Isotopic
587 constraints on water balance and evapotranspiration partitioning in gauged watersheds across
588 Canada, *Journal of Hydrology: Regional Studies*, 37, 100878,
589 <https://doi.org/10.1016/j.ejrh.2021.100878>, 2021.

590 Grant, G. E., and Dietrich, W. E.: The frontier beneath our feet, *Water Resour. Res.*, 53,
591 2605-2609, <https://doi.org/10.1002/2017WR020835>, 2017.

592 Hughes, C. E., and Crawford, J.: A new precipitation weighted method for determining the
593 meteoric water line for hydrological applications demonstrated using Australian and global
594 GNIP data, *J. Hydrol.*, 464-465, 344-351, <https://doi.org/10.1016/j.jhydrol.2012.07.029>, 2012.

595 Kleine, L., Tetzlaff, D., Smith, A., Wang, H., and Soulsby, C.: Using water stable isotopes to
596 understand evaporation, moisture stress, and re-wetting in catchment forest and grassland soils
597 of the summer drought of 2018, *Hydrol. Earth Syst. Sci.*, 24, 3737-3752,
598 <https://doi.org/10.5194/hess-24-3737-2020>, 2020.

599 Koeniger, P., Gaj, M., Beyer, M., and Himmelsbach, T.: Review on soil water isotope-based
600 groundwater recharge estimations, *Hydrol. Process.*, 30, 2817-2834,
601 <https://doi.org/10.1002/hyp.10775>, 2016.

602 Landwehr, J. M., and Coplen, T. B.: Line-conditioned excess: a new method for characterizing
603 stable hydrogen and oxygen isotope ratios in hydrologic systems, *International conference on
604 isotopes in environmental studies*, 2006, 132-135, 2006.

605 Landwehr, J. M., Coplen, T. B., and Stewart, D. W.: Spatial, seasonal, and source variability in the
606 stable oxygen and hydrogen isotopic composition of tap waters throughout the USA, *Hydrol.
607 Process.*, 28, 5382-5422, <https://doi.org/10.1002/hyp.10004>, 2014.

608 Li, X., Piao, S., Wang, K., Wang, X., Wang, T., Ciais, P., Chen, A., Lian, X., Peng, S., and
609 Peñuelas, J.: Temporal trade-off between gymnosperm resistance and resilience increases forest
610 sensitivity to extreme drought, *Nature Ecology & Evolution*, 4, 1075-1083,
611 <https://doi.org/10.1038/s41559-020-1217-3>, 2020.

612 Liu, Y., Liu, F., Xu, Z., Zhang, J., Wang, L., and An, S.: Variations of soil water isotopes and
613 effective contribution times of precipitation and throughfall to alpine soil water, in Wolong
614 Nature Reserve, China, *Catena*, 126, 201-208, <https://doi.org/10.1016/j.catena.2014.11.008>,
615 2015.

616 Ma, X., Jia, W., Zhu, G., Ding, D., Pan, H., Xu, X., Guo, H., Zhang, Y., and Yuan, R.: Stable
617 isotope composition of precipitation at different elevations in the monsoon marginal zone,
618 *Quatern. Int.*, 493, 86-95, <https://doi.org/10.1016/j.quaint.2018.06.038>, 2018.

619 McCutcheon, R. J., McNamara, J. P., Kohn, M. J., and Evans, S. L.: An evaluation of the
620 ecohydrological separation hypothesis in a semiarid catchment, *Hydrol. Process.*, 31, 783-799,
621 <https://doi.org/10.1002/hyp.11052>, 2017.

622 Milly, P. C. D.: Climate, soil water storage, and the average annual water balance, *Water Resour.*
623 *Res.*, 30, 2143-2156, <https://doi.org/10.1029/94WR00586>, 1994.

624 Pang, Z., Kong, Y., Froehlich, K., Huang, T., Yuan, L., Li, Z., and Wang, F.: Processes affecting
625 isotopes in precipitation of an arid region, *Tellus B: Chemical and Physical Meteorology*, 63,
626 352-359, <https://doi.org/10.1111/j.1600-0889.2011.00532.x>, 2011.

627 Penna, D., Hopp, L., Scandellari, F., Allen, S. T., Benettin, P., Beyer, M., Geris, J., Klaus, J.,
628 Marshall, J. D., Schwendenmann, L., Volkmann, T. H. M., von Freyberg, J., Amin, A.,
629 Ceperley, N., Engel, M., Frentress, J., Giambastiani, Y., McDonnell, J. J., Zuecco, G., Llorens,
630 P., Siegwolf, R. T. W., Dawson, T. E., and Kirchner, J. W.: Ideas and perspectives: Tracing
631 terrestrial ecosystem water fluxes using hydrogen and oxygen stable isotopes – challenges and
632 opportunities from an interdisciplinary perspective, *Biogeosciences*, 15, 6399-6415,
633 <https://doi.org/10.5194/bg-15-6399-2018>, 2018.

634 Penna, D., Stenni, B., Šanda, M., Wrede, S., Bogaard, T. A., Michelini, M., Fischer, B. M. C.,
635 Gobbi, A., Mantese, N., Zuecco, G., Borga, M., Bonazza, M., Sobotková, M., Čejková, B., and
636 Wassenaar, L. I.: Technical Note: Evaluation of between-sample memory effects in the analysis
637 of $\delta^2\text{H}$ and $\delta^{18}\text{O}$ of water samples measured by laser spectrometers, *Hydrol. Earth*
638 *Syst. Sci.*, 16, 3925-3933, <https://doi.org/10.5194/hess-16-3925-2012>, 2012.

639 Peralta-Tapia, A., Sponseller, R. A., Tetzlaff, D., Soulsby, C., and Laudon, H.: Connecting
640 precipitation inputs and soil flow pathways to stream water in contrasting boreal catchments,
641 *Hydrol. Process.*, 29, 3546-3555, <https://doi.org/10.1002/hyp.10300>, 2015.

642 Qu, D., Tian, L., Zhao, H., Yao, P., Xu, B., and Cui, J.: Demonstration of a memory calibration
643 method in water isotope measurement by laser spectroscopy, *Rapid Commun. Mass Sp.*, 34,
644 e8689, <https://doi.org/10.1002/rcm.8689>, 2020.

645 Rothfuss, Y., and Javaux, M.: Reviews and syntheses: Isotopic approaches to quantify root water
646 uptake: a review and comparison of methods, *Biogeosciences*, 14, 2199-2224,
647 <https://doi.org/10.5194/bg-14-2199-2017>, 2017.

648 Sharma, H., Ehlers, T. A., Glotzbach, C., Schmid, M., and Tielbörger, K.: Effect of rock uplift and
649 Milankovitch timescale variations in precipitation and vegetation cover on catchment
650 erosion rates, *Earth Surf. Dynam.*, 9, 1045-1072, <https://doi.org/10.5194/esurf-9-1045-2021>,
651 2021.

652 Snelgrove, J. R., Buttle, J. M., Kohn, M. J., and Tetzlaff, D.: Co-evolution of xylem water and soil
653 water stable isotopic composition in a northern mixed forest biome, *Hydrol. Earth Syst. Sci.*, 25,
654 2169-2186, <https://doi.org/10.5194/hess-25-2169-2021>, 2021.

655 Sprenger, M., Leistert, H., Gimbel, K., and Weiler, M.: Illuminating hydrological processes at the

656 soil-vegetation-atmosphere interface with water stable isotopes, *Rev. Geophys.*, 54, 674-704,
657 <https://doi.org/10.1002/2015RG000515>, 2016.

658 Sprenger, M., Llorens, P., Cayuela, C., Gallart, F., and Latron, J.: Mechanisms of consistently
659 disjunct soil water pools over (pore) space and time, *Hydrol. Earth Syst. Sci.*, 23, 2751-2762,
660 <https://doi.org/10.5194/hess-23-2751-2019>, 2019.

661 Sprenger, M., Tetzlaff, D., and Soulsby, C.: Soil water stable isotopes reveal evaporation
662 dynamics at the soil–plant–atmosphere interface of the critical zone, *Hydrol. Earth Syst. Sci.*,
663 21, 3839-3858, <https://doi.org/10.5194/hess-21-3839-2017>, 2017.

664 Tang, K., and Feng, X.: The effect of soil hydrology on the oxygen and hydrogen isotopic
665 compositions of plants' source water, *Earth Planet. Sc. Lett.*, 185, 355-367,
666 [https://doi.org/10.1016/S0012-821X\(00\)00385-X](https://doi.org/10.1016/S0012-821X(00)00385-X), 2001.

667 Tetzlaff, D., Soulsby, C., Buttle, J., Capell, R., Carey, S. K., Laudon, H., McDonnell, J., McGuire,
668 K., Seibert, J., and Shanley, J.: Catchments on the cusp? Structural and functional change in
669 northern ecohydrology, *Hydrol. Process.*, 27, 766-774, <https://doi.org/10.1002/hyp.9700>, 2013.

670 Xiao, W., Wei, Z., and Wen, X.: Evapotranspiration partitioning at the ecosystem scale using the
671 stable isotope method—A review, *Agr. Forest Meteorol.*, 263, 346-361,
672 <https://doi.org/10.1016/j.agrformet.2018.09.005>, 2018.

673 Yin, L., Dai, E., Zheng, D., Wang, Y., Ma, L., and Tong, M.: What drives the vegetation dynamics
674 in the Hengduan Mountain region, southwest China: Climate change or human activity? *Ecol.*
675 *Indic.*, 112, 106013, <https://doi.org/10.1016/j.ecolind.2019.106013>, 2020.

676 Zhu, G., Yong, L., Zhang, Z., Sun, Z., Sang, L., Liu, Y., Wang, L., and Guo, H.: Infiltration
677 process of irrigation water in oasis farmland and its enlightenment to optimization of irrigation
678 mode: Based on stable isotope data, *Agr. Water Manage.*, 258, 107173,
679 <https://doi.org/10.1016/j.agwat.2021.107173>, 2021a.

680 Zhu, G., Yong, L., Zhang, Z., Sun, Z., Wan, Q., Xu, Y., Ma, H., Sang, L., Liu, Y., Wang, L., Zhao,
681 K., and Guo, H.: Effects of plastic mulch on soil water migration in arid oasis farmland:
682 Evidence of stable isotopes, *Catena*, 207, 105580, <https://doi.org/10.1016/j.catena.2021.105580>,
683 2021b.

684 Zimmermann, U., Münnich, K. O., Roether, W., Kreutz, W., Schubach, K., and Siegel, O.: Tracers
685 Determine Movement of Soil Moisture and Evapotranspiration, *Science*, 152, 346-347,
686 <https://doi.org/10.1126/science.152.3720.346>, 1966.